



ELSEVIER

Journal of Electron Spectroscopy and Related Phenomena 124 (2002) 225–243

JOURNAL OF
ELECTRON SPECTROSCOPY
and Related Phenomena

www.elsevier.com/locate/elspec

Dynamics of excited electrons in metals, thin films and nanostructures

M. Bauer*, M. Aeschlimann

Department of Physics, University of Kaiserslautern, 67663 Kaiserslautern, Germany

Received 5 December 2001; received in revised form 18 January 2002; accepted 20 February 2002

Abstract

The immense progress in the field of ultrashort pulsed lasers made it possible to study ultrafast dynamics of photoexcited hot electrons in metals by means of a variety of pump-probe techniques. Time-resolved two-photon photoemission has the capability of directly monitoring the dynamics of electrons with specific energy and momentum during the course of the transformation of a nascent (as photoexcited) nonthermal electron distribution to an excited Fermi–Dirac distribution. The main purpose of this investigation was to gain a basic understanding of the dynamics of single excited electrons at a metal surface, particularly in an energy region which is important for surface photochemistry and catalytic model reactions ($E_F < E < E_{\text{vac}}$). In these studies, the roles of secondary electrons and transport effects in equal pulse cross-correlation experiments were considered. The results demonstrate the feasibility of studying electron relaxation in noble and transition metals as a function of band structure, spin-polarization, surface morphology and dimensionality. We also present an extension of the common time-resolved two photon photoemission method to higher energies ($h\nu > 20$ eV, UPS mode) and high lateral resolution (PEEM mode). © 2002 Elsevier Science B.V. All rights reserved.

Keywords: Electron dynamics; Ultrafast spectroscopy; Surface science; Magnetism

1. Introduction

In many modern fields such as fs-photochemistry and (magneto)electronics, an understanding of rate limiting processes can be elucidated by studies of the dynamics of photoexcited hot electrons. In the case of metals where the unoccupied electronic states are not restricted by a band gap, hot electrons relax directly into thermal equilibrium with the whole electron gas, randomizing both their energy and momentum. The lifetime of individual excited elec-

tronic states in metals is always short, typically on the order of only a few femtoseconds (fs) and, hence, a detailed study of relaxation phenomena in the time domain has just begun. In general, carrier–phonon interaction and luminescence play minor roles in the energy relaxation of hot electrons in metals. Only at energies close to the Fermi level, where the inelastic lifetime increases rapidly, does electron–phonon scattering become more important. At low excited carrier density, the dominant hot electron relaxation process is inelastic scattering of the excited electrons with electrons of occupied states at and below the Fermi level, leaving both electrons in excited states above the Fermi level. Defects, impurities and, for polycrystalline samples, grain boundaries will in-

*Corresponding author. Tel.: +49-631-205-2816; fax: +49-631-205-3903.

E-mail address: mkbauer@physik.uni-kl.de (M. Bauer).

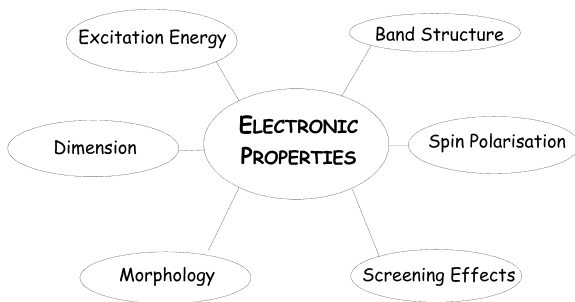


Fig. 1. The dynamic properties of photoexcited electrons are governed by a variety of intrinsic and extrinsic parameters.

crease the elastic scattering rate but typically have a negligible effect on the inelastic scattering rate of bulk electronic excitations [1]. The electron–electron scattering process in a metal is determined by the complicated competition between the phase space available for the transitions and the screening effects of the electron plasma. Unfortunately, no mathematically rigorous method of treating many-body effects in most real metals exists. One must rely on different intuitive approximations and hope that they contain the important physics of the properties being investigated.

In this paper, we will show that the lifetime of electronic excitations in metals depends on the excitation energy, screening effects, band structure, spin polarization, dimensionality of the system, and the morphology of the sample (Fig. 1). The data are obtained by means of time-resolved two-photon photoemission (TR-2PPE), based on the equal pulse correlation technique. Combined with ultra-fast laser techniques, TR-2PPE is one of very few techniques that enable one to study the state of the electron system during the course of its transformation from a nascent nonthermal electron distribution to an excited Fermi–Dirac distribution. By using state-of-the-art laser technology, it is possible to investigate electron dynamical processes at surfaces with a time-resolution of a few femtoseconds [2–5].

2. Theory

Early theoretical approaches were based on the Landau theory of Fermi liquids (FLT) which treats the excitation as a quasiparticle [6,7]. The lifetime

τ_{ee} of a single particle excitation of an electron gas, as determined by electron–electron interactions, can be calculated from the imaginary part Σ_1 of its self energy $\Sigma(\vec{p})$. Quinn and Ferrell treated this problem in a theoretical study considering a Fermi liquid-like free electron gas [8]. In the case of low excitation energies $E(\vec{p})$ and when the effect of plasmon creation can be excluded ($E(\vec{p}) \ll \hbar\omega_p$), they derived the following formula for E_1 [7]

$$\Sigma_1(\vec{p}) = -\frac{e^2}{2\pi^2} \int_{E_F}^{E(\vec{p})} \frac{d^3\vec{q}}{q^2} \frac{\varepsilon_2(\vec{q}, \Delta E(\vec{q}))}{|\varepsilon(\vec{q}, \Delta E(\vec{q}))|^2} \quad (1)$$

where $\varepsilon = \varepsilon_1 + i\varepsilon_2$ is the complex dielectric function of the electron gas and $\Delta E(\vec{q})$ is the energy transfer through the interaction of the excited electron with the electron gas at momentum exchange \vec{q} . The decay time of the excitation is then given by

$$\tau_{ee} = \frac{1}{2|\Sigma_1(\vec{p})|} \quad (2)$$

The integrand in Eq. (1), $\frac{\varepsilon_2}{|\varepsilon|^2} = \text{Im}\left(-\frac{1}{\varepsilon}\right)$, is referred to as the bulk energy loss function. This expression can be derived by considering the power loss of a charged particle due to the dielectric shift inside a bulk [9]. Consequently, $E_1(\vec{p})$ results from the sum of all possible decay channels of an electron provided by the interaction with the electron gas. In detail, ε_2 serves as a measure of the number of states available for real transitions due to interaction with the electron gas, whereas the denominator accounts for the screening of these interactions by the electron plasma. It is the competition between transitions and screening which ultimately determines the lifetime of an excitation.

Quinn suggested that the screening of electron–electron interactions is adequately included in the Thomas–Fermi dielectric function $\varepsilon^{\text{TF}}(\vec{q}, \Delta E(\vec{q}) = 0)$ if the energy of the excited electron $E(p)$ is close enough to the Fermi energy E_F [7]. In this case, the denominator of Eq. (1) can be replaced by

$$\varepsilon(\vec{q}, \Delta E(\vec{q})) \cong \varepsilon^{\text{TF}}(\vec{q}, 0) = 1 + \frac{q_s^2}{q^2} \quad (3)$$

$$q_s^2 = 4 \cdot (3/\pi)^{1/3} \cdot \frac{n^{1/3}}{a_0}$$

where q_s is the inverse Thomas–Fermi screening length, n the density of the electron gas and a_0 the Bohr radius. This approach considers that the system is always in equilibrium with respect to screening. The electron gas reacts instantaneously to changes induced by interactions with the excited electron and screens such disturbances within a typical length of $1/q_s$.

Under these conditions, Quinn derived the following simple expression for the lifetime τ_{ee} in a 3D system which is known as Fermi-liquid behavior (FLT):

$$\tau_{ee} = \tau_0 \cdot \frac{E_F^2}{(E - E_F)^2} \quad (4)$$

The prefactor τ_0 is primarily determined by the free electron density n and is approximately given by [10]

$$\tau_0 \approx \frac{64}{\sqrt{3} \cdot \pi^{5/2}} \cdot \frac{\sqrt{m}}{e} \cdot \frac{1}{\sqrt{n}}$$

If we take into account that the Fermi energy E_F is also a function of the electron density, then the dependence of τ_{ee} can be given as

$$\tau_{ee} = \text{const} \cdot \frac{n^{5/6}}{\delta E^2}$$

According to these assumptions, the inelastic lifetime of an excited electron as a function of its excitation energy δE with respect to the Fermi edge E_F is determined by the density of the electron gas.

This theory is only strictly valid for a Fermi liquid-like free electron gas. However, Quinn showed that the relaxation process of a degenerate nearly free electron gas in metallic conducting bands may still be in a reasonable quantitative agreement with the FLT within certain limits [7]. However, even in noble metals, the role of the screening interaction between extended sp and localized d electrons has to be taken into account [11–13]. Recently, several first-principles calculations of hot electron lifetimes in real solids have been performed that quantitatively account for the interplay between band structure and many-body effects on electron relaxation processes [14–17]. In general, the ab initio results for Cu and Au are slightly larger than the simple jellium (free electron gas) results obtained

with the FLT. For Ag, the agreement between both theories is even better. This can be explained by the fact that the Fermi surface of Ag is nearly spherical. Only for energies smaller than 1 eV, the FLT lifetimes are higher. Since aluminum is a simple metal with no d-bands, the hot-electron lifetime should be well described within a free-electron model. However, due to a lattice-induced splitting of the band structure above the Fermi level new decay channels are opened, decreasing the hot electron lifetime [15,16,18].

3. Experimental methods

3.1. Time-resolved two-photon photoemission technique

The experimental method used to investigate the lifetime of electronic excitations of metallic conducting bands is time-resolved two-photon photoemission (TR-2PPE), a direct measurement of dynamical properties in the time domain with a resolution of a few femtoseconds. The principle is schematically shown in Fig. 2. An ultrashort pump laser pulse excites electrons out of the valence band of the metal within the optical penetration depth of the surface. The transient population of the intermediate excitation is probed by a second ultrashort laser pulse which promotes the still excited electrons to the vacuum where their energy is analyzed. Information about the depopulation time of the intermediate state and, hence, the average lifetime of a single excited electron in a certain energetic state is obtained by varying the time delay between pump and probe pulses.

3.2. Experimental set-up

Our time-resolved two-photon photoemission experiments were carried out with an 82 MHz pulsed Ti:Sapphire laser, tunable from 750 to 830 nm. The system delivers transform-limited and sech^2 temporally-shaped pulses of up to 9 nJ/pulse with a duration of 20–40 fs. As shown in Fig. 3, the linearly polarized output is frequency doubled in a 0.15-mm-thick Beta Barium Borate (BBO) crystal to produce UV pulses at $h\nu = 3.0\text{--}3.4$ eV. The beam is

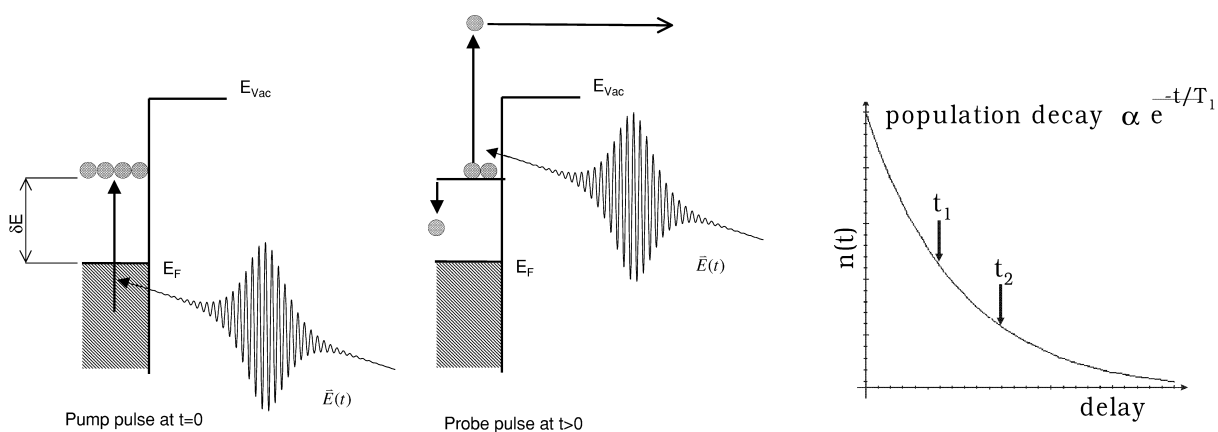


Fig. 2. The time-resolved two-photon photoemission process.

sent through a pair of fused silica (GVD) to pre-compensate for pulse broadening due to dispersive elements such as lenses, beam-splitters and the UHV-chamber window in the optical path. The pulses are split by a beam splitter to equal intensity (pump and probe pulses), and one path is delayed with respect to the other by a computer-controlled delay stage. Both beams are combined collinearly by a second beam splitter and are focused at 45° incidence on the sample surface. In an autocorrelation set-up the same photon energy and polarization is used for both pulses and therefore the detected autocorrelation

trace (2PPE intensity vs. pump-probe delay time) is symmetric with respect to time zero (temporal overlap of the pulses). By using two different polarizations (p- and s-polarized) or different photon energies the symmetry in time is broken. For the investigation of the lifetime of electronic volume states, we typically use the equal pulse cross-correlation techniques (pump and probe are equal in photon energy and intensity, but have different polarization) in order to minimize coherent effects between the pump and probe pulse.

The samples are mounted in an UHV-chamber

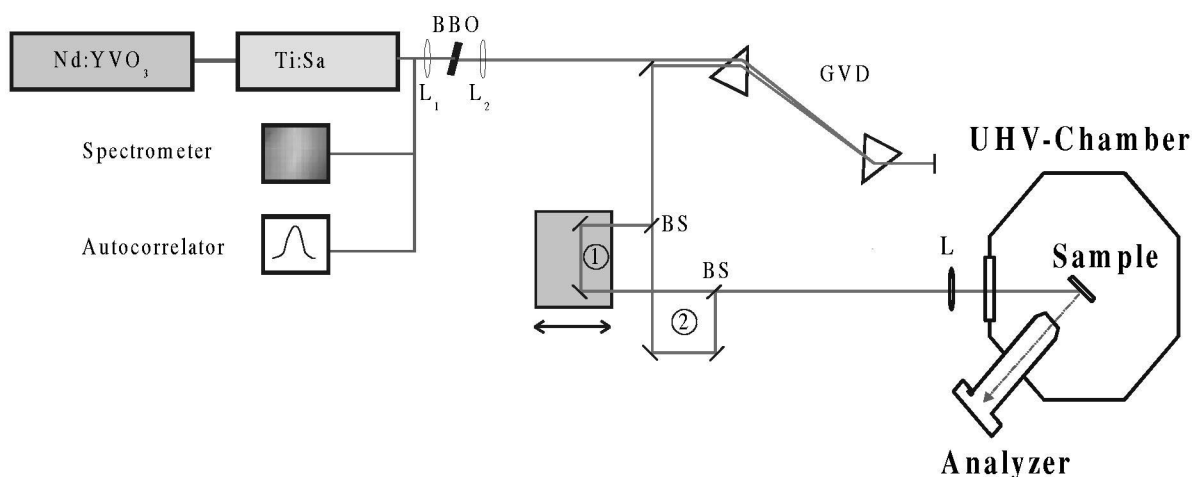


Fig. 3. Set-up for a time-resolved 2PPE experiment.

(base pressure 8×10^{-11} mbar) equipped with a cylindrical sector electron energy analyzer. In general, we use a pass energy of 4 eV, leading to roughly 50 meV resolution. A 4.0 V bias is applied to the sample to eliminate the effects of any stray electric fields. The samples (single crystals and polycrystalline films) were prepared by several sputtering and heating cycles. Sample cleanliness was checked using work function measurements, as determined by the onset of the 2PPE spectra, and Auger spectroscopy, and compared with the respective literature data. For some measurements, cesium was deposited onto the sample surface by evaporation from a commercial getter source to lower the work function. This enabled us to extend the accessible energy range to excitation energies down to 0.5 eV above E_F . The effect of Cs on electron scattering is negligible in the case of a crosspolarized experiment. Within the present time-resolution, we did not observe any difference in the lifetime measurements on a clean metal surface compared to a Cs/metal surface in the overlapping energy region.

By using a low pulse energy (< 0.3 nJ/pulse) and a high-repetition-rate laser, we avoid space-charge effects that can distort the measured photoelectron spectrum. The count rate is much less than one electron per pulse. Assuming a spot size of ~ 150

μm , we estimate a pulse fluence of typically $1.5 \mu\text{J}/\text{cm}^2$ at the sample surface under these conditions (temporal and spatial overlap).

3.3. The different read-out models

Fig. 4 shows a typical 2PPE spectrum of a polycrystalline silver foil probed by only one beam. The spectrum carries the signature of the electronic band structure, the photon energy, and the lifetime of the intermediate state. A longer lifetime increases the cross-section for the absorption of a second photon. As seen in the inset, the energy δE of the intermediate state E_j above E_F is given by: $\delta E = E_j - E_F = E_{\text{vac}} + E_{\text{kin}} - h\nu$, where E_{kin} represents the detected kinetic energy of the photoelectron, E_{vac} symbolizes the work function of the sample, and $h\nu$ is the photon energy. The pump-probe experiments are carried out by monitoring the number of electrons at a given kinetic energy E_{kin} as a function of delay between the pump and probe pulses (two pulse correlation experiment). Fig. 5 shows a cross-correlation trace from a Ta sample at an intermediate state energy $\delta E = 3.0$ eV. The background originates from emitted electrons excited by photons from a single pulse (see left and right sides of Fig. 5). The nonlinear character of two-photon photoemission

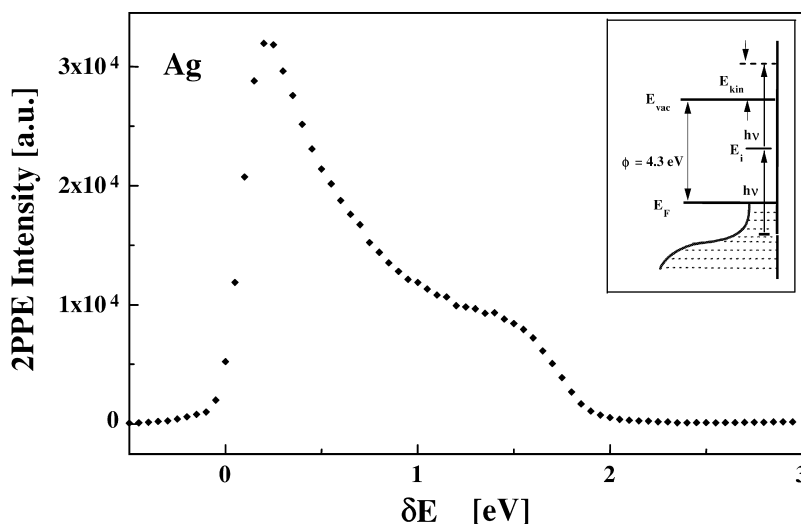


Fig. 4. Two-photon photoemission spectrum of the flat Ag-valence band. The yield increases at lower energy due to the enhanced lifetime and cascade processes.

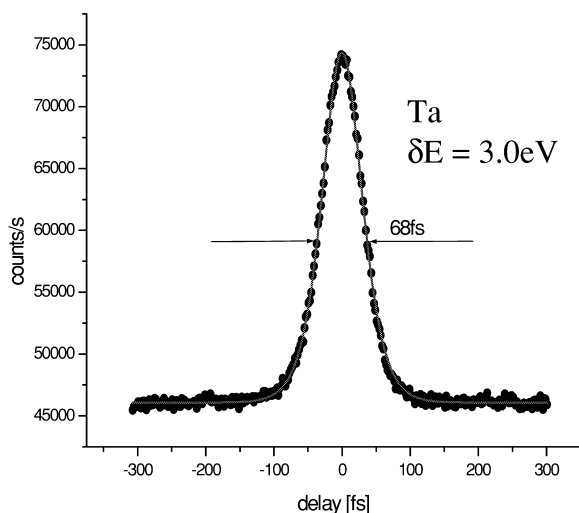


Fig. 5. Measured equal pulse cross-correlation trace obtained by 2PPE from a Ta sample at $\delta E = 3.0$ eV.

(2PPE is a second-order process) leads to an increase in the 2PPE yield when the pulses are spatially and temporally superimposed, as seen at $\Delta t = 0$ in Fig. 5. As long as the two laser pulses temporally overlap, an electron can be emitted by absorbing just one photon from each pulse. When the pulses are temporally separated an excited electron from the first pulse is still able to absorb a photon from the second pulse as long as the inelastic lifetime of the intermediate state exceeds the delay.

An experimental effect on the signal is caused by the finite pulse width of our probe. Therefore, two pulse correlation data are, in fact, the results of a complicated convolution of the actual signal (decay function) with the pump and probe pulses. The most plausible and straightforward method for comparing electron relaxation phenomena with theoretical hypotheses would be to compare measurements of experimental data points with simulated relaxation curves. By assuming a simplified mechanism prior to the numerical evaluation, calculated points can be constructed. The sum of the squared differences from the measured points can then be minimized to obtain least-squares estimates for the dynamical parameters (e.g. T_1 and T_2 , see below) that are contained in the model. However, one should be careful in interpreting the experimental traces; the simplest mechanism (e.g. a mono-exponential decay, cf. Fig. 2), which is

sufficient to fully describe the convoluted 2PPE-traces, is not necessarily the correct one. For some traces one can easily obtain a nearly perfect fit of an oversimplified mechanism to the convoluted traces. This also means that—unless independently obtained evidence would support a particular mechanism—parameters estimated from pump-probe results are to be regarded only within the framework of that particular mechanism and not as generally valid characteristics of the fast and complicated electron relaxation process on a metal surface.

For interpretation of the observed time response we used a density matrix formalism which accounts for energy and phase relaxation in a three-level system on a phenomenological basis (Fig. 6). For the propagation of the density matrix we use the Liouville-von Neumann equation. This equation follows the common formalism of a density matrix and can be seen as a quantum mechanical attempt to describe the interaction of an electronic system with an electromagnetic field [19]:

$$\frac{d}{dt}\rho = -\frac{i}{\hbar}[H, \rho] + \frac{d}{dt}\rho^{\text{diss.}} \quad (5)$$

Here the density matrix ρ is defined by $(\rho)_{nm} = |n\rangle\langle m|$ where n and m denote the different electron states. The diagonal elements $(\rho)_{nn}$ give the probability of the system being in state $|n\rangle$, while $(\rho)_{nm} = (\rho)_{mn}^*$ represent the optically-induced coherence

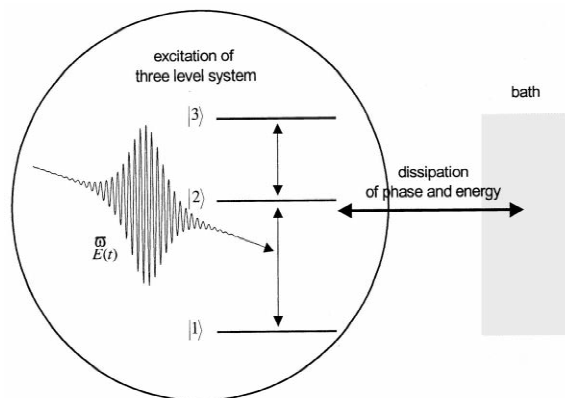


Fig. 6. System considered within the used density matrix formalism. The disturbing Hamiltonian operator is given by the interaction of a three-level system with an electromagnetic field. The dissipative terms are determined by the coupling to an external bath.

between $|n\rangle$ and $|m\rangle$. The dissipative term $d/dt\rho^{\text{diss}}$ describes the temporal decay of the respective elements of the density matrix due to coupling to an external bath. The interaction with this reservoir gives rise to energy and phase loss processes, described by the population decay time T_1 and the dephasing time T_2 , respectively.

The potential of the Liouville-von Neumann formalism for describing the three-step excitation mechanism of TR-2PPE was shown by Hertel et al., who achieved a consistent description of the spectroscopy (2PPE) and dynamics (TR-2PPE) of the ($n=1$) image-potential states on a Cu(111) surface [20]. Also Bauer et al. successfully demonstrated the capability of that formalism in their investigations of photoexcited alkali chemisorbates [21]. In addition, Ogawa et al. succeeded in simulating the non-resonant excitation of an image-potential state, as obtained by means of interferometric TR-2PPE [22]. The three-level model is, in principle, exactly valid for describing a system of three discrete states. Hence, the Liouville-von Neumann formalism is a simplified representation of the real excitation process between electron bands in a metal. Weida et al. have shown in a recent publication that effects due to continuum excitation in a metallic band lead to an attenuation of the oscillatory envelope, which drastically influences the reconvoluted dephasing time T_2 but do not affect the measured inelastic lifetime T_1 [23].

In the case of a pure three-level system one obtains a set of nine coupled differential equations. Five free parameters are left, i.e. the decay of the population of state $|2\rangle$ and $|3\rangle$ and the dephasing of all three states (Fig. 6). The number of free parameters is further reduced by the following assumptions: (i) decay and dephasing of state $|3\rangle$ is set to zero (inverse LEED state), (ii) dephasing of state $|1\rangle$ and $|2\rangle$ is chosen as <2 fs. In the case of bulk electron excitations in metals as investigated in this publication, and under our experimental conditions (excitation pulse length), rapid dephasing of the excitation process is a reasonable assumption. This reduces Eq. (5) to the well-known rate equation model for a population $N(t, E)$ of the intermediate state:

$$\frac{d}{dt}N(t, E) = A(t, E) - \frac{1}{\tau_{\text{ee}}}N(t, E) \quad (6)$$

Here $A(t, E)$ is excitation-induced by the first (pump)

laser pulse and $\tau_{\text{ee}}(E) = T_1$ the measured energy-dependent relaxation time of the electron population in the intermediate state $|2\rangle$.

3.4. Secondary electrons and transport effect

TR-2PPE probes the population decay of excited electrons in a defined energy range resolution range, limited by the finite energy resolution of the electron analyzer. Since the systems and the experimental modes are complex, we have to carefully consider any additional processes besides the decay process that might contribute to our measured signal. On one hand, mixing of different processes might be considered as a disturbance. On the other hand, we should be aware that any additional contribution to our signal contains information about the system. Two processes that give rise to additional contributions to our TR-2PPE signal are the creation of secondary electrons following the primary excitation process induced by the laser, and transport of electrons away from the probed surface region into the bulk.

3.4.1. Secondary processes

In addition to the photo-excitation of electrons into the probed intermediate state, excited electron populations may be further increased by secondary processes as a consequence of the primary excitation. This is caused either by: (i) inelastic decay of excited electrons from energetically higher-lying states (cascade process) or (ii) relaxation of excited holes, created during the primary excitation process by means of an Auger decay.

According to Quinn, the electron loses about 66% of its excitation energy during a typical collision [7]. Ritchie mentioned that this value decreases to 50% if one takes the anti-symmetry of the electron's wave function into account [24]. At a typical photon (excitation) energy of $h\nu = 3.3$ eV, the highest excited state probed in an experiment will be 3.3 eV above the Fermi level. Therefore, refilling processes due to cascade processes in an energy range between 2 and 3.3 eV should have only a minor effect on our experiment. In addition Eq. (4) suggests relaxation times in the range of only a few femtoseconds at the high energy end, i.e. about 3 eV in our experiment. Considering the strong lifetime dependence which is proportional to $1/\delta E^2$, refilling should be instant-

neous with respect to the intrinsic lifetime of the state, even for excitations as low as 2 eV above E_F , and should not significantly disturb the interpretation of our results to a great extent. For lower excitation energies, however, the effect on the refilling of an energetic population by cascades increases and might become substantial. Hence, in this energy range, the measured relaxation time can be dominated by cascade processes rather than by the lifetime of a single excited electron.

Another source of secondary electrons is the relaxation of the photoinduced holes by means of an Auger decay. If the dynamical properties of the electronic system are symmetric with respect to the Fermi edge in the exchange of the electron and the hole, then such a process should compete with the measured decay channel on the same time scale as the electron-induced secondary electrons, e.g. a minor effect on high energy excitations with an increasing disturbance of excitations close to the Fermi edge.

One approach for including these secondary processes in a theoretical description of the 2PPE process would be to expand, for example, the rate-equation model corresponding to the intermediate state to

$$\frac{d}{dt}N(t, E) = A(t, E) - \frac{1}{\tau_{ee}}N(t, E) + C(t, E) + D(t, E) \quad (7)$$

where $C(t, E)$ accounts for refilling due to the cascade electrons and $D(t, E)$ for refilling due to electrons created by Auger decay of holes. Unfortunately, primary excitations and secondary processes are essentially indistinguishable in an experiment. The strong deviation of measured cross-correlation traces from model simulations, as observed by Hertel et al. at a copper surface in a bichromatic TR-2PPE experiment [3], might indicate such secondary processes. Simulations of cross-correlation traces, taking these secondary processes into account, have confirmed this interpretation [25,26]. The experimental data supported our assumption that the deviations caused by these refilling processes become important at about half the maximum excitation energy and increase further as the Fermi edge is approached.

3.4.2. Transport effect

The second factor which must be taken into account is transport of the photoexcited electrons away from the probed surface region. In our experiment, this will reduce the photoelectron intensity emitted by the probe pulse out of the surface region and will set a lower limit for measured lifetimes by TR-2PPE. For example, even if the electrons had an infinitely long lifetime, there should still be an experimentally measurable decrease in the photoelectron yield as a function of pump-probe delay time due to the electron moving away from the surface and out of the probe volume. Using a simple approach, we might assume that a separate mechanism is responsible for decay and transport and, therefore, sum the measured decay rates in correspondence with Matthiessen's rule

$$\frac{1}{T_{\text{meas.}}} = \frac{1}{\tau_{ee}} + \frac{1}{T_{\text{trans.}}} \quad (8)$$

leading in any case to $T_{\text{meas.}} < \tau_{ee}$. Hence, the depletion of an excited state population in the probed region as a function of the time delay between the two pulses depends on the intrinsic decay of the excited energetic state *and* on transport.

Model calculations of the transport effect on copper have been carried out by Schmuttenmaer et al. [2] using a ballistic model and by Knoesel et al. [27], who took explicit band structure of different copper surfaces into account. As expected from Eq. (8), transport may actually induce a strong deviation (reduction) of the measured lifetime compared to the intrinsic inelastic lifetime, depending on the ratio between $T_{\text{trans.}}$ and τ_{ee} . The calculation made by Schmuttenmaer et al. suggests a value of 30 fs for $T_{\text{trans.}}$. Based on this model, which assumes the electron transport inside the bulk to be ballistic, 30 fs can be taken as the lower limit for $T_{\text{trans.}}$. Any scattering process causes the electron to become confined within the surface region, increasing the effective transport time. Our own recent experimental and theoretical investigations (based on the Boltzmann equation) of thin noble metal films evaporated on insulator substrates actually indicate the importance of this transport effect [26]. However, it should be noted that these considerations are based on a model implying static sample conditions. Fem-

tosecond pump-probe experiments induce a highly dynamical situation within the investigated material where these assumptions may no longer be applicable. It is for this reason that, e.g. Ekardt and coworkers questioned the existence of the transport effect in femtosecond time-resolved 2PPE experiments [28].

4. Experimental results and discussion

In this section, we present TR-2PPE measurements selected to demonstrate that the lifetime of electronic excitation in metals depends on the excitation energy, screening effects, band structure, spin polarization, dimensionality of the system, and the morphology of the sample.

4.1. Excitation energy, screening effect, and bandstructure

Fig. 7 shows the lifetimes determined from the correlation traces of the TR-2PPE measurements as a function of the electrons' excitation energy $\delta E = E - E_F$ for a thin noble-metal film (silver, 30 nm thick) and three transition metal films (iron, 20 nm; nickel, 40 nm; and cobalt, 10 nm). There are three points which we would like to emphasize:

- (i) The lifetime of optically excited electronic states in metals is short, typically in the order of only few femtoseconds for $\delta E > 1.5$ eV.
- (ii) The lifetime, and hence, inelastic mean free path is strongly energy-dependent. All curves show a clear increase in the relaxation time τ as E_F is approached. This trend can be explained by the fact that, according to conventional Landau Fermi liquid theory, the available phase space for scattering of an excited electron with electrons from the 'cold' Fermi sea is proportional to $1/\delta E^2$.
- (iii) The data show that the lifetimes for transition metals iron, nickel and cobalt are substantially shorter than in silver. This can be explained with a phase space argument. In comparison with the noble metal silver, where the d-band is completely filled and localized well below the Fermi energy, the d-bands of transition metals crosses

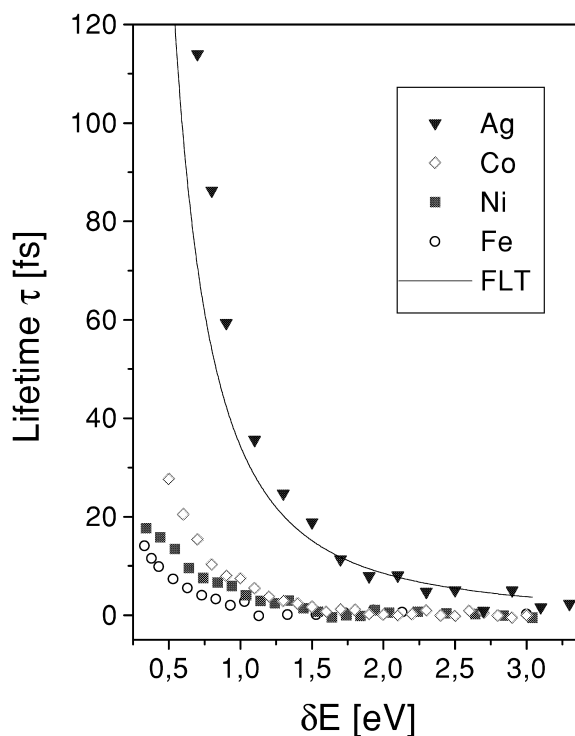


Fig. 7. Measured relaxation times of excited electrons in different metals plotted versus the energy of the electrons measured from the Fermi energy. The solid line shows the Fermi liquid values for Ag.

E_F and, hence, are only partially filled. Consequently, the available phase space for electron–electron scattering is increased. This shows that the relaxation is dominated to a considerable degree by the density of the occupied and unoccupied states near E_F .

For transition metals, excitations of the strongly bonded d-electrons near E_F do not allow a qualitative agreement with the Fermi-liquid theory (prefactor, see Eq. (4)). The monovalent noble metal silver, however, seems to meet most of the requirements for a degenerate, free electron gas. However, there may be deviations from free electron behavior due to the d-bands, located well below the Fermi edge but still within the conducting band. Enhanced screening as well as additional decay channels from, for example, interband transitions due to the excitation of electrons from the d-band into the sp-band, may be the

result of this additional electronic structure. The onset of the d-band of silver at 4 eV below E_F makes this electron system the most suitable Fermi liquid system of all the noble metals. At the excitation energies δE below 3.4 eV, these states cannot be involved in the decay process of the excited electrons, at least with respect to interband transitions. And indeed, the agreement with the Fermi-liquid theory (solid line, $r_s = 2.47$, $E_F = 8.22$ eV, see Ref. [17]) is evident. However, we still have to consider transport effects in the 30-nm-thick film as will be shown below.

4.2. Film thickness dependence of the relaxation time τ

All the data points in Fig. 7 were plotted without considering transport of the excited carriers out of the surface region into the bulk as discussed in Section 3.4. For transition metals, the lifetime in the

investigated energy range is too short for transport to play a role, but that might not be the case for silver. As long as refilling processes (secondary electrons) can be neglected, it should be possible to reduce or even eliminate transport effects using films as thin as the penetration depth of the laser light.

The relaxation of photoexcited electrons as a function of energy for thin Ag-films with thicknesses of 15, 20 and 30 nm are shown in Fig. 8. For comparison, the bulk value of Ag is also shown. The epitaxial Ag(100) thin films were grown on air cleaved MgO(100) single crystal substrates under ultra high vacuum and monitored in-situ by LEED. The MgO(100) single crystals were transferred into a UHV chamber immediately after cleaving and cleaned by heating to 1300 K for at least 4 h. The epitaxial Ag(100) films were grown on these substrates at room temperature. The thickness of the film was controlled by a quartz crystal microbalance. This procedure results in smooth, well-defined and orien-

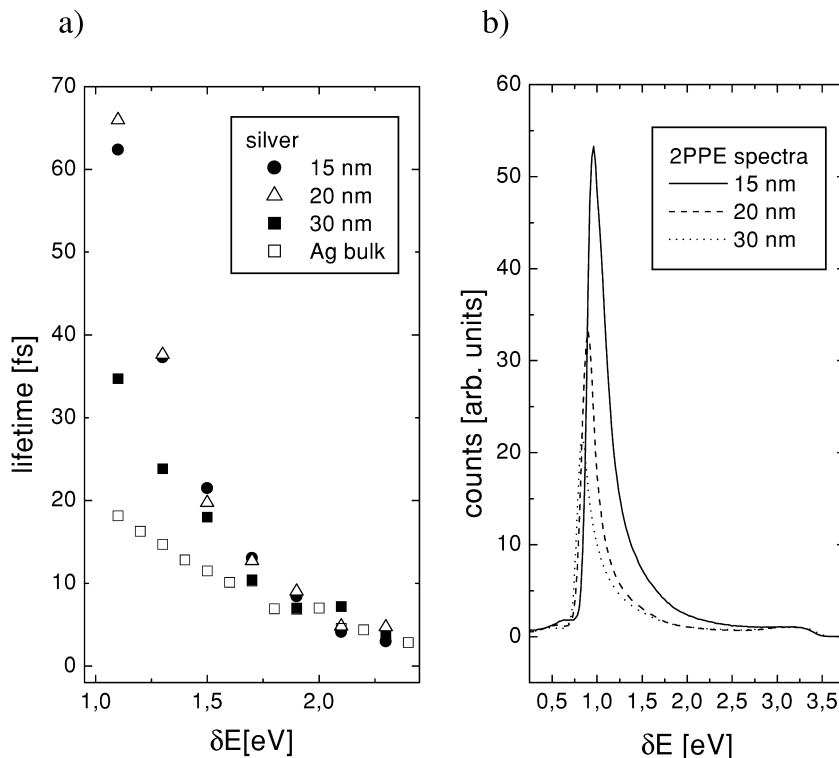


Fig. 8. (a) Measured relaxation times of excited electrons plotted versus the energy above the Fermi level for three different Ag film thicknesses. For comparison, the bulk value of Ag is also shown. (b) 2PPE spectra for the three different film thicknesses.

tated Ag(100) electrodes with sharp LEED patterns. The photon energy used for these measurements was 3.3 eV. A clear difference in the measured relaxation is visible below $\delta E < 1.6$ eV, indicating that in this energy range, both the energetic decay of the optically excited electrons and transport reduce the number of detectable photoelectrons. In Fig. 8b, the 2PPE-intensities for all three films are shown. A distinct reduction in intensity with increasing film thickness is observed, caused by strong diffusion of the excited electrons out of the probed surface region. For the thinner films the potential barrier, set up by the insulating substrate on the reverse side of the sample, reduces or even eliminates this diffusion effect and traps the excited electrons within the probed surface area. The intensity change is only apparent for lower excitation energies and hence longer inelastic lifetimes, where the electron mean free path starts to exceed the respective film thickness. Interestingly, we see also an increase in the 2PPE intensity for a 15-nm film compared to the 20-nm film, where we actually cannot find any difference in the measured lifetime. These experimental data support the intuitive assumption that the transport of excited electrons into the bulk affects the measured lifetime in a TR-2PPE experiment. Depending on the investigated energy region, it has either no influence (high excitation energies) on the experimental data or it dominates the measured relaxation dynamics (low excitation energies in the case of silver).

In comparison with the FLT, the real lifetime for silver is the lifetime of the thin film, where any transport effect can be excluded. Therefore, the prefactor for silver is slightly higher than that predicted by the FLT theory. For the data points above 1.5 eV, the relaxation time may be increased by increasing the refilling processes of the investigated electronic states due to secondary electrons as discussed in Section 2. The increased lifetime for silver compared to FLT is in full agreement with the ab initio calculation by Keyling et al. [17].

4.3. Spin-dependent electron dynamics in ferromagnets

In Section 4.1, we have shown that the relaxation is dominated to a considerable degree by the density

of the occupied and unoccupied states near E_F . Due to the exchange splitting in ferromagnetic materials, the density of the occupied and unoccupied states near E_F is different for the two spin states of the electron. Hence, the inelastic lifetime τ of electrons excited in ferromagnetic materials should be different for majority-spin (\uparrow) and minority-spin (\downarrow) electrons. This has been discussed in the literature for a number of years, but despite the fundamental nature of a spin-dependent lifetime, the ratio $\tau^\uparrow/\tau^\downarrow(E)$ has never been measured directly in a ferromagnetic material. Initial evidence that $\tau^\uparrow \neq \tau^\downarrow$ stems from measurements such as the enhancement of secondary electron spin polarization at low kinetic energies [29–32]. More direct experimental information is based on spin-resolved overlayer experiments which investigate the spin-dependent transmission of electrons through ultrathin ferromagnetic metal films [33,34]. Spin-dependent relaxation has important implications, e.g. the interpretation of spin-polarized spectroscopy of ferromagnetic materials must take into account a spin-dependent transport of excited electrons to the surface, known as the spin filter effect [30].

Using time domain measurements, the inelastic lifetime T_1 rather than the mean free path of the excited electrons is probed. This may be more appropriate for investigating the spin-dependent dynamics of excited electron relaxation mechanisms. Adding a spin analyzer to the electron energy analyzer of a conventional time-resolved 2PPE setup makes the separate but simultaneous measurement of both spin states possible. The electrons at a fixed energy are counted according to their spin in two different channeltrons as a function of the time-delay between the two pulses for a given magnetization direction. To compensate for an apparatus-induced asymmetry, the magnetization is then reversed and the measurement is taken again. From the resulting four datasets, the relaxation times τ^\uparrow and τ^\downarrow for spin-up and spin-down electrons are extracted using the same deconvolution method as discussed above. Each pair of data points presented in the plots of this section is the average of 8–10 single relaxation time measurements.

Spin-dependent relaxation effects will be superimposed on the spin integrated (unpolarized) relaxation time. Therefore, a spin dependence in the relaxation

time can only be observed if the spin-integrated relaxation time can be temporally resolved in our experiment. As shown in Fig. 7, in the energy range above 1.4 eV, we find for all three transition metals relaxation times below our temporal resolution (<2 fs). On the other hand, at intermediate state energies close to E_F , the electrons emitted by 1PPE processes start to become important. They induce a large background to the 2PPE signal and make an accurate extraction of the lifetimes difficult. Therefore, spin-resolved measurements can only be usefully performed for intermediate state energies between 0.3 and 1.1 eV.

In Fig. 9, the spin-dependent relaxation time for electrons of Fe, Co, and Ni films are plotted. The error bars in the plot represent the statistical scatter. The experimental results of the three examined ferromagnetic materials show two common facts: (i) the lifetime for majority-spin electrons is always

found to be longer than the lifetime for minority-spin electrons and (ii) the value for $\tau^\uparrow/\tau^\downarrow$ lies between 1 and 2. We observe the largest differences between τ^\uparrow and τ^\downarrow for Ni and Co, whereas for Fe, the difference is slightly reduced. This qualitative behavior of the spin-dependent lifetime can be readily explained by the excess of unfilled minority-spin states compared to unfilled majority-spin states. According to this simple model, the spin-dependence of the scattering rate is larger for the strong ferromagnets Co and Ni than for the weak ferromagnet Fe. This is in agreement with our measurements, where only a small spin-effect could be detected for iron. In Fe, this model would even predict a reversal of the effect for low energies below 1 eV, i.e. the lifetime for spin-down electrons should become longer than the lifetime for spin-up electrons. A ratio of $\tau^\uparrow/\tau^\downarrow$ below 1 is, however, not observed for $E - E_F < 1$ eV. This indicates that the simple model,

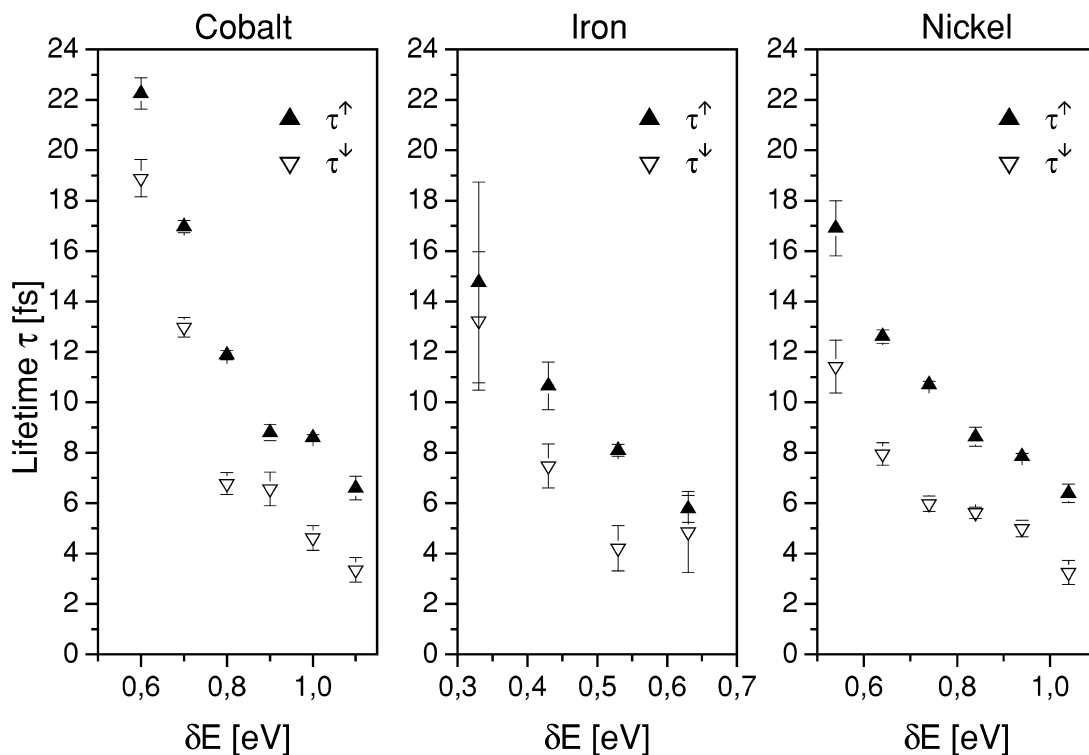


Fig. 9. Spin-resolved relaxation times for fcc Co(100), bcc Fe(100) and Ni(100) films. For all three ferromagnets, the population of excited minority-spin electrons decays faster than that of majority-spin electrons within the investigated energy range.

considering the different number of empty electronic states as the only decisive factor for a spin-dependent relaxation time, is not adequate for a quantitative interpretation of our experimental data.

4.4. Effect due to a change in the surface morphology

In metal nanoparticles, collective electronic oscillations—the so-called Mie-plasmons—can be excited by light and are, therefore, detectable as a pronounced optical resonance in the visible or UV parts of the spectrum. In recent years, several linewidth measurements and time resolved SHG autocorrelation measurements on metallic (Au, Ag) nanoparticles have been published, reporting a dephasing time T_2 (also often called decay or damping time) of the localized particle plasmon excitation in the order of 8–20 fs [35–37].

Much less is known about the physical mechanism underlying the dephasing time T_2 . Depending on the size, size distribution, shape, dielectric constant of the surrounding medium etc., the following potential mechanisms are: First, the plasmon can decay by pure dephasing, e.g. a decay of the fixed phase correlation between the individual electronic excitations of the whole oscillator ensemble, described by a pure dephasing time T_2^* . Additional mechanisms may be scattering on surfaces or simple decay of the collective mode due to inhomogeneous phase velocities caused by the spread of the excitation energy or the local inhomogeneity of the nanoparticles. The

plasmon can also decay due to a transfer of energy into quasi-particles (electron-hole pairs) or reemission of photons (radiation damping and luminescence), described by T_1 .

We focus on the study of elliptically-shaped metal nanoparticles with semi-axes of 40 by 80 nm and a height of 45 nm. Silver nanoparticles are of special interest as they can exhibit particularly strong size-dependent optical extinction in the visible spectral range (1.8–3 eV) due to resonantly driven electron plasma oscillations.

Elliptic-shaped metal nanoparticles show two different plasmon resonances which lie at different wavelengths for light polarized parallel to the short and long axes, respectively. Tuning the laser wavelength to one of these two resonances allows us to distinguish between resonance excitation and off-resonance excitation (both are intraband processes) by simply changing the polarization of the laser pulse.

The samples investigated were produced in the group of Professor Aussenegg, Karl-Franzens University in Graz. The two-dimensional array of nearly identical, parallel oriented silver particles are deposited lithographically on a transparent ITO substrate which itself lies on a glass plate. Fig. 10 illustrates the geometry, size and the distances of the particles in the array. In the following, the long half axis of the elliptic particle is called ‘a’ and the short half axis is called ‘b’. The whole square array containing the particles has a size of 200 μm lateral length. Electron beam lithography was used to define

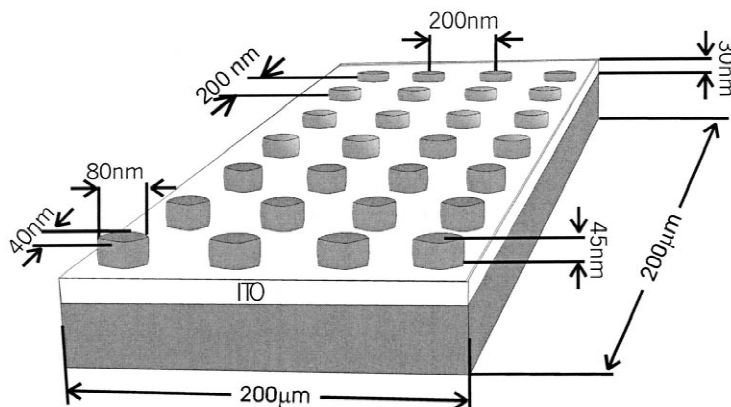


Fig. 10. Array of silver-nanoparticles deposited on ITO.

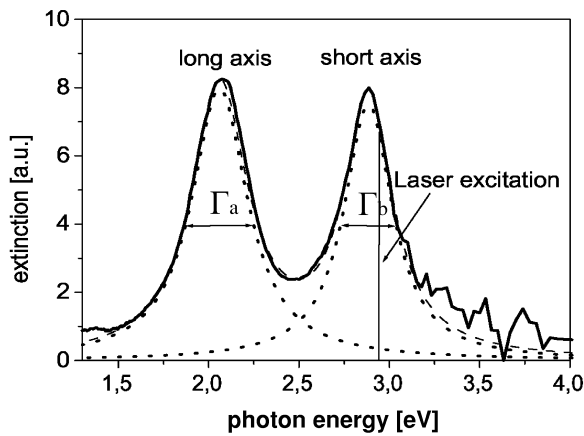


Fig. 11. Measured extinction spectrum of the nanoparticle array. The low- and high-frequency peaks correspond to the Mie plasmons excited along the long and short axes of the elliptical Ag particles, respectively.

the metallic nanoparticles [38,39]. As particle shape and interparticle distance can be varied independently, this method allows us to tailor the optical properties of single particles. Thus the resonance frequency and the strength of particle interactions can be changed independently. Thereby the optical extinction maximum can be tuned to the desired wavelength (in this case to the illuminating laser wavelength of 415 nm).

Fig. 11 shows the two different resonances in the extinction spectrum at $\omega_a = 2.1$ eV and $\omega_b = 2.95$ eV. Liebsch predictions that the Mie plasmon damping is nearly independent of the resonance frequency [40] is in good agreement with the measured FWHM of the peaks in the extinction spectrum as shown in Fig. 11. For the long axis, $\Delta E(\text{FWHM}) = 0.4$ eV and for the short axis, $\Delta E(\text{FWHM}) = 0.39$ eV.

In Fig. 12, the FWHM derived from the auto-

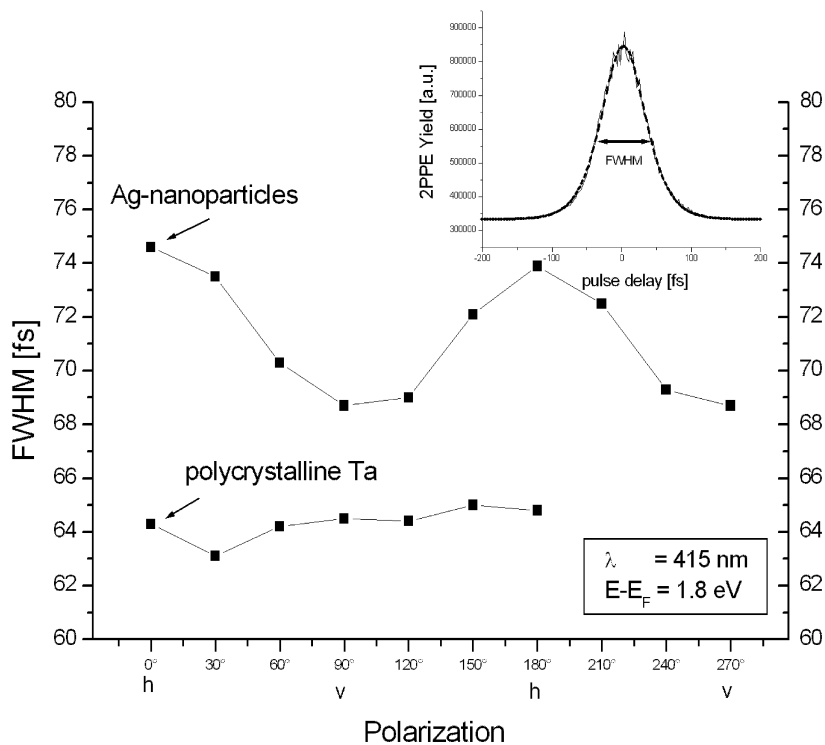


Fig. 12. Nanoparticles show a variation of the FWHM of the autocorrelation over rotating states of polarization while tantalum shows no effect. In the inset, a typical autocorrelation measurement can be seen from which the data points have been derived.

correlation 2PPE traces are plotted as a function of the state of polarization relative to the long axis (h). For comparison, the behavior of polycrystalline tantalum is also shown. The FWHM for tantalum is not affected by rotating the polarization angle of the incoming light. Therefore, any effect caused by an increase in the dispersion due to rotation of the half wave plate can be excluded. For the elliptical Ag-nanoparticles, however, a rotation of 90° reduces the FWHM from almost 75 fs in the 'b' direction (short-axis mode, resonant plasmon excitation) to 69 fs in the 'a' direction (long-axis mode, off-resonant plasmon excitation). Further rotation of the polarization to the long axis restores the long lifetime of the plasmon excitation. One should be aware that these FWHM values still include the autocorrelation of the laser pulse width. The autocorrelation traces of tantalum were measured at an intermediate state energy $E - E_F = 2.8$ eV. In this energy range, the lifetime of excited electrons in a transition metal is less than 1 fs (Fig. 7) and hence, the traces obtained for tantalum represent the pure laser autocorrelation curve. Any increase in the FWHM in the autocorrelation measurement for Ag nanoparticles compared to the Ta values must be caused by a lifetime effect of the optically excited electron system. It might be tempting to conclude from the FWHM results of Fig. 12 that on-resonance collective excitation in general has a longer lifetime than excitation far from resonance. According to Liebsch and co-workers [40], the different damping rates obtained under on- and off-resonance conditions, as shown in Fig. 12, can also be explained by different magnitudes of radiation damping along the short and long axis of the elliptical particles. This result is consistent with the well-known fact that for spherical particles, radiation losses become more pronounced with increasing radius. Surface scattering plays a role only at radii less than about 5 nm. Moreover, Liebsch's theory predicts that collective plasma oscillations within the nano-particles are subject to the same microscopic Drude damping processes due to phonons, impurities, electron–electron interactions as off-resonance excitations [40]. None of these inelastic scattering mechanisms is reduced or absent if the electrons oscillate near the resonance excitation.

5. Outlook

Over the last decade, TR-2PPE has become a useful experimental method to study dynamical processes of optically excited electrons on ultrashort time-scales. These results are meant to be representative of experiments performed by an increasing number of groups in this field.

In the last section of this paper, we will present two novel time-resolved methods based on the combination of femtosecond laser systems with conventional surface analytical techniques. In particular, we will demonstrate the potential of time-resolved PEEM (photoemission electron emission microscopy) and time-resolved UPS (ultraviolet photoemission spectroscopy). The experiments on TR-PEEM are a result of a collaboration with the group of Professor Schönhense at the University of Mainz, whereas the TR-UPS experiment has been set up in the group of Professor Murnane and Professor Kapteyn at JILA/Colorado by one of the authors (M. Bauer) during his postdoctoral period.

5.1. TR-PEEM

Over the last decade, there have been numerous attempts to combine scanning probe microscopy and femtosecond pump-probe techniques to realize an ultrafast microscope with nanometer resolution [41]. To our knowledge, no satisfactory solution has yet been presented. Our idea is to combine femtosecond laser sources and a spatial resolving photoemission technique (PEEM), to achieve this goal [42]. In this way we are able to overcome one of the main problems of TR-SPM which is the interaction of the intense laserfield with the probe (e.g. tip, cantilever) itself. The experimental scheme is almost identical to a time-resolved 2PPE set-up (Fig. 3). The only difference is that the energy discriminating electron analyzer is replaced by a spatial (and optionally energy) resolving photoemission electron microscope. For a pump-probe scan, the PEEM-images are taken at different temporal delays between pump and probe. Thus, for each image pixel an autocorrelation trace is measured, representing the actual lifetimes corresponding to electrons emitted from a specific location on the sample. In this preliminary study, our

goal was to prove the principle of this experimental technique, that is, the observation of lifetime contrast on a structured surface. The sample of choice for this test phase was a GaAs substrate covered with a periodic array of silver hexagons of microscopic dimensions (Fig. 13a). The area between the hexagons left exposed interstitial GaAs. Whereas lifetimes of optical excited electrons in metals lie typically in the range of some tenths of femtoseconds as has been shown above, the restricted phase space for electron–electron scattering in semiconductors as imposed by the existence of the bandgap, gives rise to lifetimes of up to hundreds of femtoseconds (at excitation energies > 1 eV above the conduction band minimum) [43]. Thus, even in an energy integrating mode, as used in this test phase experiment, sufficient lifetime contrast is achieved. Fig. 13(a) shows the static PEEM image as obtained by regular threshold photoemission using a Hg-vapor lamp. Image (b) represents the same observed by two photon photoemission using our fs-laser source. Image (c) is the corresponding lifetime contrast image obtained from a 2PPE pump-probe scan. The brightness value of a pixel corresponds to the FWHM of the autocorrelation trace and is an indirect measure of the electron lifetime. The observed contrast between the metallic and semiconductor surfaces can be identified with the different dynamics in the two materials. Note that in the center of the image (c), essentially no contrast can be observed between silver and GaAs in correspondence with an

enhanced photoemission yield in Fig. 13 (a) and (b). This might be the result of contamination of the GaAs interstitial part with small silver clusters in this boundary area as a result of the evaporation process. In particular, for small silver particles, effective coupling of the exciting laser light to localized plasmons can enhance photoemission yields quite significantly.

These first results demonstrate that the device is capable of visualizing lateral variations in the hot electron lifetime on heterogeneous microstructured sample surfaces. In general, this method offers a new contrast method for PEEM by the use of a femtosecond pulsed light source. Even more importantly, this technique is capable of examining the characteristics of hot-electron dynamics on surfaces at a potential spatial resolution of a few nanometers and a time resolution of a few femtoseconds. In particular, we expect that this technique is a new probe for the physics of charge carriers in nanostructured and low-dimensional systems (see also Ref. [44]).

5.2. TR-UPS

Up to this point, this paper has dealt exclusively with methods used to probe the dynamics of electron excitations at surfaces. This experimental method may prove its use in the study of the surface electronic dynamics that govern chemical surface reactions. We pose the ultimate question: Would it also be possible to monitor the chemical reaction

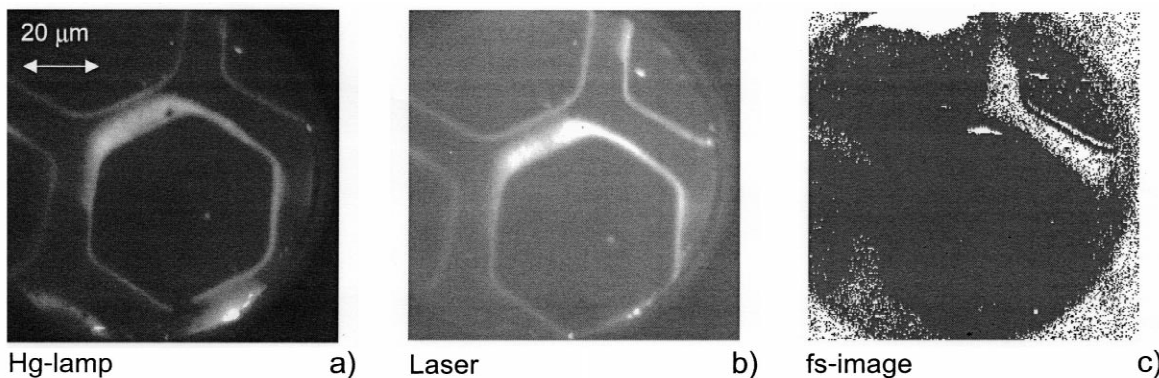


Fig. 13. TR-2PPE microscopy of silver on gallium arsenide. (a) PEEM image of the micro-structured Ag layer (partly visible hexagonal patches) taken with a mercury vapor UV lamp. (b) Image of the same area taken with the laser. (c) FWHM image extracted from a pump probe scan. The brightness value of each pixel corresponds to the FWHM of the respective autocorrelation trace.

itself on the time-scale of the nuclear motion of e.g. a dissociation process? Fundamental time-scales of chemical reactions are assumed to lie in the range of vibration periods of chemical bonds, some tens to a few hundreds of femtoseconds. A very promising technique is time-resolved UPS: An ultrashort pump-pulse initiates a chemical reaction at the surface, e.g. a change in the chemical state. At a certain time-delay Δt a photoemission spectrum is recorded, reflecting the chemical state at Δt by means of changes in the valence states (UPS). Successive change in Δt will finally give a series of photoemission spectra representing—like a movie—the entire repeatable part of the course of the chemical reaction. The challenging part of this experiment is the pulsed photon source delivering photon energies of at least >20 eV at a pulsewidth of a few tenths of femtoseconds and at sufficient flux. Pulsewidth of third generation synchrotrons are in the range of 100 ps and even pulses from next generation synchrotrons will still be in the picosecond timescale, not capable of achieving the required time-resolution. Recently, another technique to produce VUV light has attained much interest, the technique of high harmonic generation. The interaction of an intense laserfield with atoms (typically noble gases) can lead to quite efficient generation of ultrashort photon pulses in the EUV and XUV energy range. Maximum photon energies close to 1 keV have been reported to date [45]. Theoretically and experimentally it has been shown that the pulsewidth of such a source can lie in the sub-femtosecond regime [46]. In a recent experiment it was possible to observe the change in chemical state of molecular oxygen adsorbed on a Pt(111) surface by combining high harmonic generation and photoemission spectroscopy [47]. The experiment is shown in Fig. 14. We use an amplified Ti:Sapphire laser system that generates 1.4 mJ, 800 nm, 25 fs pulses at 1-kHz repetition rate. The output is split into two pulses (20%/80%) where one part initiates the excitation of the oxygen (Pump). The major part of the split pulse is used to generate the (high harmonic) UV probe pulses. An energy of 40.5 eV (27th harmonic), selected by a multilayer mirror, is used to probe the chemical state of the oxygen via the valence states of the adsorbate-surface system. The sample is mounted in an UHV-chamber and held at a temperature of 77 K. One saturation layer of

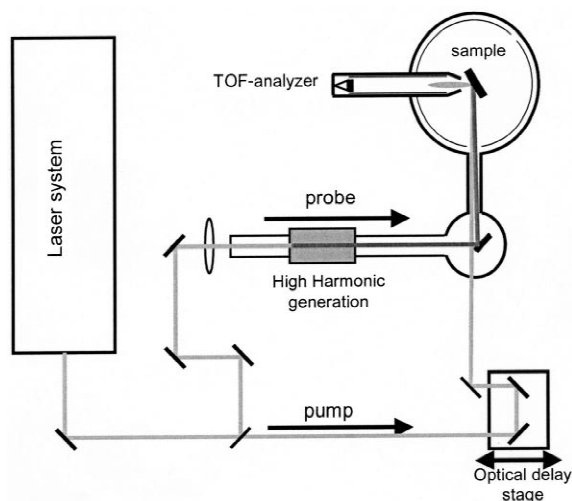


Fig. 14. Experimental set-up for femtosecond time-resolved UPS using High Harmonics.

molecular oxygen is adsorbed on the surface. The excitation of oxygen under these conditions (30 fs pump pulse, absorbed flux: 1 mJ/cm^2) occurs via transfer processes of hot electrons from the substrate. The response of such an excitation as reflected in the UPS spectrum is shown in Fig. 15. The figure represents the low energy part of the valence band at binding energies of about 11 eV to 3 eV with respect to E_F . The left spectrum is taken without being pumped as a reference. At time-zero (b) (temporal overlap between pump and probe) no change in the spectral part of interest can be observed; 250 fs later (c), however, a peak appears at a binding energy of about 6 eV. It is even stronger at about 500 fs (d). In order to clarify that this observation is not the result of a permanent change in the sample, another scan at time zero is taken (e) which is essentially identical to (b). More detailed scans reveal that the population of this excited state takes about 550 fs (Fig. 16). From comparison with static measurements as well as theoretical work, the spectral changes can be clearly related to a change in the chemical state of the adsorbed oxygen. The data are interpreted in terms of a transient excitation from a superoxo state of the molecular oxygen into a peroxo state which goes along with a reversible reorientation of the molecule into the direction of the new transient equilibrium

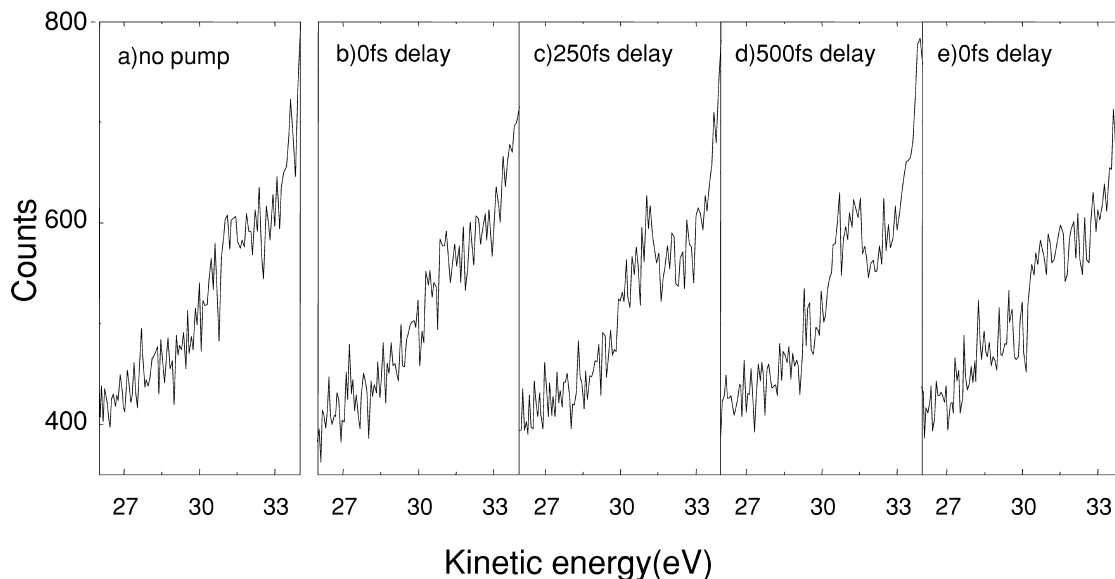


Fig. 15. Time-resolved photoemission spectra from a saturation layer of molecular oxygen adsorbed on a Pt(111) surface: (a) no pump beam; (b) with pump beam, zero delay between pump and probe; (c) 250 fs delay between pump and probe; (d) 500 fs delay between pump and probe; (e) repeat of (b), taken immediately after (d).

position. This would account for the observed temporal delay of the appearance of the peak with respect to time-zero. To our knowledge, these are the first results where the nuclear motion of a chemical reaction on a metal surface could be monitored in a real time experiment.

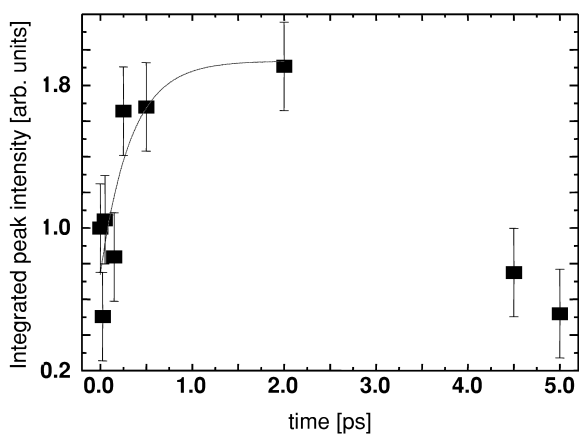


Fig. 16. Integrated amplitude of the transient valence band feature (Fig. 15) as a function of pump-probe delay. A fit of the data indicates an onset of 550 ± 140 fs.

Acknowledgements

The authors would like to acknowledge all co-workers who have impacted so much on the work reported here, in particular: S. Pawlik, R. Burgermeister, H.C. Siegmann, D. Oberli, W. Weber, R. Porath, T. Ohms, M. Scharte, J. Beesley, M. Wessendorf, O. Schmidt, C. Wiemann, O. Andreyev, G. Schönhense, C. Lei, K. Read, R. Tobey, J. Gland, M.M. Murnane, and H.C. Kapteyn. We thank B. Lamprecht, H. Ditlbacher, J.R. Krenn and F.R. Aussenegg for providing us with many Ag-nanoparticle samples. We are grateful to M. Wolf, H. Petek, P. Echenique, R. Knorren, K.H. Bennemann, and A. Liesch for many helpful discussions. This work was supported by the Swiss National Science Foundation and by the Deutsche Forschungsgemeinschaft.

References

- [1] Due to the very restricted phase space for inelastic scattering processes in front of surfaces, the modification of the electronic density of states due to surface defects might lead

- to a significant contribution to the inelastic decay of surface located states such as image potential states (W. Weinelt, Ch. Reß, M. Kutschera, U. Thomann, I.L. Shumay, Th. Fauster, U. Höfer, F. Theilmann, A. Goldmann, Appl. Phys. B 68 (1999) 377–381; M. Weinelt, Appl. Phys. A 71 (2000) 493).
- [2] C.A. Schmuttenmaer, M. Aeschlimann, H.E. Elsayed-Ali, R.J.D. Miller, D.A. Mantell, J. Cao, Y. Gao, Phys. Rev. B 50 (1994) 8957.
 - [3] T. Hertel, E. Knoesel, M. Wolf, G. Ertl, Phys. Rev. Lett. 76 (1996) 535.
 - [4] M. Aeschlimann, M. Bauer, S. Pawlik, Chem. Phys. 205 (1996) 127.
 - [5] S. Ogawa, H. Nagano, H. Petek, Phys. Rev. B 55 (1997) 10869.
 - [6] N.W. Ashcroft, N.D. Mermin, Solid State Physics, Saunders College, New York, 1976.
 - [7] J.J. Quinn, Phys. Rev. 126 (1962) 1453.
 - [8] J.J. Quinn, R.A. Ferrell, Phys. Rev. 112 (1958) 812.
 - [9] Ch. Kittel, Introduction into Solid State Physics, Wiley, New York, 1986.
 - [10] D. Pines, P. Nozieres, The Theory of Quantum Liquids, Benjamin, New York, 1966.
 - [11] E. Zarate, P. Apell, P.M. Echenique, Phys. Rev. B 60 (1999) 2326.
 - [12] C. López Bastidas, J.A. Maytorena, A. Liebsch, Phys. Rev. B 65 (2001) 035417.
 - [13] P.J. van Hall, Phys. Rev. B 63 (2001) 104301.
 - [14] I. Campillo, J.M. Pitarke, A. Rubio, E. Zarate, P.M. Echenique, Phys. Rev. Lett. 83 (1999) 2230.
 - [15] W.D. Schöne, R. Keyling, M. Bandic, W. Ekardt, Phys. Rev. B 60 (1999) 8616.
 - [16] I. Campillo, V.M. Silkin, J.M. Pitarke, E.V. Chulkov, A. Rubio, P.M. Echenique, Phys. Rev. B 61 (2000) 13484.
 - [17] R. Keyling, W.D. Schöne, W. Ekardt, Phys. Rev. B 61 (2000) 1670.
 - [18] M. Bauer, S. Pawlik, M. Aeschlimann, Proc. SPIE 3272 (1998) 201.
 - [19] R. Loudon, The Quantum Theory of Light, Oxford University Press, Oxford, 1973, p. 20; T. Hertel, E. Knoesel, A. Hotzel, M. Wolf, G. Ertl, J. Vac. Sci. Technol. A 15 (1997) 1503.
 - [20] T. Hertel, E. Knoesel, M. Wolf, G. Ertl, Phys. Rev. Lett. 76 (1996) 535.
 - [21] M. Bauer, S. Pawlik, M. Aeschlimann, Phys. Rev. B 60 (1999) 5016.
 - [22] S. Ogawa, H. Nagano, H. Petek, A.P. Heberle, Phys. Rev. Lett. 78 (1997) 1339.
 - [23] M.J. Weida, S. Ogawa, H. Nagano, H. Petek, J. Opt. Soc. Am. B 17 (2000) 1443.
 - [24] R.H. Ritchie, J.C. Ashley, J. Phys. Chem. Solids 26 (1965) 1689.
 - [25] E. Knoesel, A. Hotzel, T. Hertel, M. Wolf, G. Ertl, Surf. Sci. 368 (1996) 76.
 - [26] M. Aeschlimann, M. Bauer, S. Pawlik, R. Knorren, G. Bouzerar, K.H. Bennemann, Appl. Phys. A 71 (2000) 1.
 - [27] E. Knoesel, A. Hotzel, M. Wolf, Phys. Rev. B 57 (1998) 12812.
 - [28] W. Ekhardt, W.-D. Schöne, R. Keyling, Appl. Phys. A 71 (2000) 529.
 - [29] J. Unguris et al., Phys. Rev. Lett. 49 (1982) 72.
 - [30] D.R. Penn, S.P. Apell, S.M. Girvin, Phys. Rev. B 32 (1985) 7753.
 - [31] E. Kisker, W. Gudat, K. Schröder, Solid State Commun. 44 (1982) 591.
 - [32] H. Hopster et al., Phys. Rev. Lett. 50 (1982) 70.
 - [33] D.P. Pappas et al., Phys. Rev. Lett. 66 (1991) 504.
 - [34] J.C. Gröbli, D. Oberli, F. Meier, Phys. Rev. B 52 (1995) R13095.
 - [35] B. Lamprecht, A. Leitner, F.R. Aussenegg, Appl. Phys. B 68 (1999) 419.
 - [36] T. Vartanyan, M. Simon, F. Träger, Appl. Phys. B. 68 (1999) 425.
 - [37] T. Klar, M. Perner, S. Grosse, G. von Plessen, W. Spirkl, J. Feldmann, Phys. Rev. Lett. 80 (1998) 4249.
 - [38] W. Gotschy, K. Vonmetz, A. Leitner, F.R. Aussenegg, Appl. Phys. B 63 (1996) 381.
 - [39] W. Gotschy, K. Vonmetz, A. Leitner, F.R. Aussenegg, Opt. Lett. 21 (1996) 1099.
 - [40] M. Scharte, R. Porath, T. Ohms, M. Aeschlimann, J.R. Krenn, H. Dittlacher, F.R. Aussenegg, A. Liebsch, Appl. Phys. B 73 (2001) 305.
 - [41] See for example: S. Weiss, D.F. Olgetree, D. Botkin, M. Salmeron, D.S. Chelma, Appl. Phys. Lett. 63 (1993) 2567; M.R. Freeman, G. Nunes Jr., Appl. Phys. Lett. 63 (1993) 2633; W. Pfeiffer, F. Sattler, S. Vogler, G. Gerber, J.-Y. Grand, R. Möller, Appl. Phys. B 64 (1997) 265.
 - [42] O. Schmidt, M. Bauer, C. Wiemann, R. Porath, M. Scharte, O. Andreyev, G. Schönhense, M. Aeschlimann, Appl. Phys. B 74 (2002) 223.
 - [43] C.A. Schmuttenmaer, C. Cameron Miller, J.W. Herman, J. Cao, D.A. Mantell, Y. Gao, R.J.D. Miller, Chem. Phys. 205 (1996) 91.
 - [44] H.A. Dürr, F. Konast, W. Eberhardt, Adv. Solid State Phys. 41 (2001) 557.
 - [45] A. McPherson, G. Gibson, H. Jara, U. Johann, T.S. Luk, I.A. McIntyre, K. Boyer, C.K. Rhodes, J. Zhou, J. Paetross, M.M. Murnane, H.C. Kapteyn, I.P. Christov, Phys. Rev. Lett. 76 (1996) 752; Ch. Spielmann, N.H. Burnett, S. Sartania, R. Koppitsch, M. Schnürer, C. Kann, M. Lenzner, P. Wobrauschek, F. Krausz, Science 278 (1997) 661.
 - [46] I.P. Christov, M.M. Murnane, H. Kapteyn, Phys. Rev. Lett. 78 (1997) 1251; M. Hentschel, R. Kienberger, C. Spielmann, G.A. Reider, N. Milosevic, T. Brabec, P. Corkum, U. Heinzmann, M. Drescher, F. Krausz, Nature 414 (2001) 509.
 - [47] M. Bauer, C. Lei, K. Read, R. Tobey, J. Gland, M.M. Murnane, H.C. Kapteyn, Phys. Rev. Lett. 87 (2001) 025501-1.